Peer-reviewed version available at Metals 2018, 8, 1021; doi:10.3390/met8121021

Article

Effects of heat treatment on morphology, texture and mechanical properties of a MnSiAl multiphase steel with TRIP behavior

A. Salinas[1], A. Artigas[1], J. Perez-Ipiña[2], F. M. Castro-Cerda[1], N. F. Garza-Montes-de-Oca[3], R. Colás[3], R. Petrov[4] and A. E. Monsalve*[1].

[1] Departamento de Ingeniería Metalúrgica, Universidad de Santiago de Chile, Av. Ecuador 3735 (9170124), Santiago, Estación Central, Chile.
[2] Grupo Mecánica de Fractura, UNComa-CONICET, Neuquén 8300, Argentina..
[3] Facultad de Ingeniería Mecánica y Eléctrica, Universidad Autónoma de Nuevo León, México.
[4] Department of Electrical Energy, Metals, Mechanical Constructions & Systems, Ghent. University, Technologiepark 903, 9052 Gent, Belgium.
* Correspondence: alberto.monsalve@usach.cl.

Abstract: The effect that the microstructure exerts on the TRIP phenomenon and on the mechanical properties in a multiphase steel was studied. Samples of an initially cold-rolled ferrite-pearlite steel underwent different intercritical annealing treatments at 750°C until an equal fractions of austenite/ferrite was reached; the intercritical treatment was followed by isothermal bainitic treatments before cooling the samples to room temperature. Samples in the first treatment were heated directly to the intercritical temperature, whereas other samples were heated to either 900 or 1100°C to obtain a fully homogenized, single phase austenitic microstructure prior to the conducting the intercritical treatment. The high temperature homogenization of austenite resulted in the decrease in its stability, so a considerable austenite fraction transformed into martensite by cooling to room temperature after the bainitic heat treatment. Most of the retained austenite transformed during the tensile tests, and as a consequence, the previously homogenized steels showed the highest UTS. In turn, the steel with a ferritic-pearlitic initial microstructure, exhibited higher ductility than the other steels and texture components that favor forming processes.

Keywords: TRIP-assisted steel, microstructure, mechanical properties.

1. Introduction

TRIP (Transformation Induced Plasticity) assisted steels belong to the Advanced High Strength Steels family, which combine high ductility and strength. The TRIP effect consists in transformation of metastable austenite into martensite during deformation [1]. The energy absorption capacity of TRIP-assisted steels make them attractive for the automotive industry. TRIP-assisted steels have a complex multiphase microstructure consisting mainly of ferrite, bainite and retained austenite. martensite and carbides can be present in some cases [2,3]. Improvements in mechanical properties of TRIP-assisted steels are related to relationships between chemical composition and microstructure (grain size, phase morphology and others) and stability of the retained austenite [4]. The stabilization of austenite at room temperature is enhanced by carbon enrichment during heat treatment [5].

There are several studies that show the effect that morphological aspects have on retained austenite and its stability against transformation [3,6-8]. Van Dijk et al. [3] noticed that the austenite volume fraction, its carbon concentration and the grain size of the retained austenite play a crucial

role in the TRIP properties as they significantly affect the mechanical stability of the retained austenite. They found that the stability of retained austenite decreases when the carbon content decreases. Other studies [6-8] reported that the increase of the grain size of the retained austenite decreases the austenite stability and, consequently, increases the TRIP effect. Wang et al. [7] relate the chemical austenite stabilization with the extra interfacial (austenite/martensite) energy required for fine austenite grains. It means, increasing austenite grain size, increasing MS temperature. Sugimoto et al. [9] studied the effects of silicon and manganese contents on volume fraction and stability of retained austenite in carbon-manganese-silicon TRIP-assisted dual-phase steels, finding that the volume fraction of retained austenite increased with the increase of silicon and manganese contents. Pereloma et al. [10] suggested that Al decreases the carbon activity coefficient in ferrite, increases the solubility of C in ferrite, at the same time inhibits the precipitation of Fe carbides leading to higher enrichment in carbon of retained austenite. However, Al increases Ms temperature, making the retained austenite less stable. They also considered that 1.5% Mn content assures hardenability in TRIP-assisted steels.

According to De Cooman [11], some alloying elements have an important influence on the TRIP-effect. Si and Al inhibit cementite formation increasing the carbon content of retained austenite because of the extremely low solubility of Si and Al in cementite. Si significantly increases the C activity coefficient in both ferrite and austenite and reduces the solubility of C in ferrite. Instead, coinciding with Pereloma et al. [10]. On the other hand, soluble Mn stabilizes austenite, decreases the activity coefficient of C in ferrite and austenite, increasing the C solubility in ferrite and it is soluble in cementite.

In a previous work on a multiphase low alloy TRIP steel, Guzmán [12] proposed that an optimum combination of microstructure and properties can be obtained with an intercritical treatment of 10 minutes at 750 °C (just above A_1), reaching an α/γ proportion near of 1/1. Matsumara et al. [13] showed that heating just above A_1 ensures a large content of retained austenite with good stability that provides for the best combination of strength and ductility.

Based on the facts that: a) the TRIP effect is significant for large austenite grain size [6-8]; b) the global mechanical response of a multiphase TRIP assisted steel is also influenced by the interaction with the other microstructural constituents; c) heat treatment has a strong influence on microstructural features, which has an effect on austenite stability (chemical and mechanical) and the features of others constituents; d) consequently an optimum heat treatment must exist that, considering both effects, maximizes mechanical properties. According to these considerations, three TRIP-assisted steels with the same chemical composition were processed in different ways, but fixing a near 1/1 proportion of austenite and ferrite during intercritical annealing. The effect of heat treatment on grain size, texture and microstructure were studied, investigating the influence of these variables on the final microstructure and mechanical properties.

2. Materials and Methods

A steel ingot was cast at the Metallurgical Engineering Department, University of Santiago, Chile (USACH), with a composition corresponding to a TRIP-assisted steel. The material was melted in a Power-Trank induction furnace and then sand cast in a 100x100x500 mm mold. The chemical composition obtained was 0.20%C, 1.88%Mn, 0.88%Si and 0.13%Al (in weight %). The ingot was homogenized and forged at 1,250°C up to 20 mm thickness. The ingot was next hot rolled at 1,100°C until reducing the thickness up to 4 mm, and then, the material was cold-rolled down to 1.50 mm, annealed and then cold rolled until obtaining a 0.87 mm thickness (42% cold working). Then, the strip was cut in three pieces that were heat treated to obtain three multiphase TRIP steels with the same chemical composition but different microstructures.

Three different processing paths were used to obtain the 1/1 (ferrite/austenite) microstructure that will be able to sustain the TRIP effect after austempering. The intercritical temperature was obtai*ned* from a previous work [12]. These paths were obtained by (i) either heating the samples to two temperatures within the fully austenitic range, followed by intercritical annealing treatment (IAT) to form equal fraction of ferrite and austenite, or (ii) were heated-up directly from room

Peer-reviewed version available at Metals 2018, 8, 1021; doi:10.3390/met8121021

temperature to the intercritical range to transform the microstructure, (cf. Fig. 1). Both paths were followed by an isothermal bainitic treatment (IBT) known also as "austempering" in a salt bath and subsequent water quenching. Fig. 1 also shows the expected microstructures at each stage. The initial microstructure, after the cold-rolling stage, is a cold worked ferrite-pearlite. A fully homogenized austenite is the microstructure prior to IAT in the austenization path. Then, two different microstructures after the IAT are obtained, as shown in Fig.1, they were denominated (F/P) and (HA) respectively. Two different homogenizing temperatures were used: 900°C (HA900) and 1100°C (HA1100). Table 1 shows the temperatures and times employed in these heat treatments.

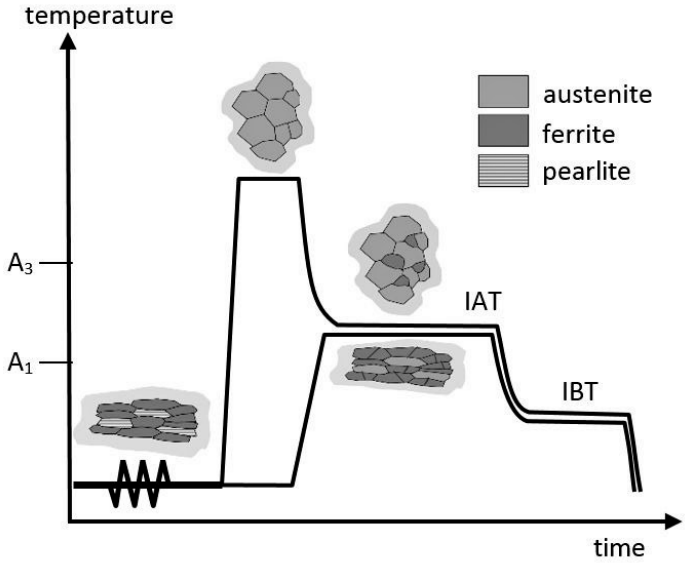

Figure 1. Schematic representation of heat treatments to obtain multiphase TRIP-assisted steels.

Table1. Parameters of the performed heat treatments and austenite grain size after austenitization.

Id. Steel	Aust. *		IAT **		IBT ***		PAGS ****
	[°C]	[min]	[°C]	[min]	[°C]	[min]	[μm]
F/P	--	--	750	10	390	7	--
HA900	900	10	750	90	390	7	10.3 ± 0.8
HA1100	1,100	10	750	135	390	7	18.9 ± 3.5

* *Austenization*
** *Intercritical Annealing Treatment*
*** *Isothermal Bainitic Treatment*
**** *Prior Austenite Grain Size (developed during the HA treatment)*

2.2. Microstructural characterization

A metallographic microscope LEICA was used to characterize the microstructures. The samples were polished and then chemically etched with a solution of 3% HNO_3 in ethanol (Nital, 3%) and LePera etchant (a 4% solution of picric acid in ethanol and a 1% solution of sodium metabisulfite in water, mixed in equal parts just before etching). Ferrite volume fraction was estimated from metallographic images by using the image analysis software ImageJ. Ferrite grain size was measured directly from metallographic images using the mean linear interception technique.

Prior austenite grain size, shown in Table 1, was measured by metallographic images after etching with a solution that contains: H_2O 25 ml, picric acid 0.3 g, hydrochloric acid 0.3 ml and as wetting agent sodium tridecylbenzene sulfonate 2.5 ml.

SEM analysis using a TESCAN Vega 3 scanning electron microscope with tungsten filament was performed at 15 kV in backscattered electron (BSE) mode.

To measure the austenite volume fraction before and after plastic deformation, X-ray measurements were carried out in a PANALYTICAL EMPYREAN diffractometer with a Co tube on samples prior and post-tensile testing. X-ray diffraction patterns were obtained in the 20°-55° 2θ range with a step (Δθ) of 0.0065° respectively. ASTM E975 method was followed to determine the austenite volume fraction in the samples. The lattice parameter was estimated using {220} FCC peaks on prior tensile test samples, and the carbon content in the retained austenite was estimated using the relationship proposed by Roberts [14].

Electron backscattered diffraction (EBSD) analyses were carried out on a plane perpendicular to the transverse direction of samples by means of the EDAX-TSL® system. A FEI XL30 ESEM microscope with a LaB6 filament was used. The specimens were analyzed on a plane tilted 70° with respect to the incidence beam at 20 kV acceleration voltage. A step size of 170 nm was used for texture analyses, whereas for microstructure characterization 60 nm step size in hexagonal scan grid was employed. EBSD data were post processed by OIM (Orientation Imaging Microscopy) Analysis™ software. The post-processing procedure included the elimination of points with low confidence index (lower than 0.1). Grains were considered with a minimum of six pixels, while grain boundaries were defined when a rotation between pixels was greater than 15°. Austenite identification by EBSD was done directly by indexation of FCC structures. Texture orientation distribution functions were calculated and represented in Bunge notation using harmonic series expansion method and imposing orthorhombic sample symmetry, series rank L=16 and a Gaussian half width of 5°.

Several authors [15,16] have suggested a EBSD based method to identify martensite regions in the EBSD scans due to their high dislocation density (10^8 cm-2 for undeformed ferrite, 10^{12} cm^{-2} for martensite) [16]. Martensite has a high density of defects and therefore, it must have a low average Image Quality (IQ) pattern [16]. An example of martensite identification criteria is explained in Fig. 2a, which shows Grain Average Image Quality (GAIQ) distributions on BCC structures for HA900 steel. It is possible to see two kinds of distribution with either high or low values of GAIQ. Martensite was assigned as units with low GAIQ values.

A second cleaning data procedure for austenite and martensite indexed data was carried out based on grain size distribution curves. An example of this is explained in Fig. 2b, which shows the retained austenite grain size distribution for HA900 steel. This picture exhibits two austenite grain size distributions. Austenite with very low grain size (lower than the threshold line) was not considered for analysis. A similar procedure was done for austenite and martensite units for each steel.

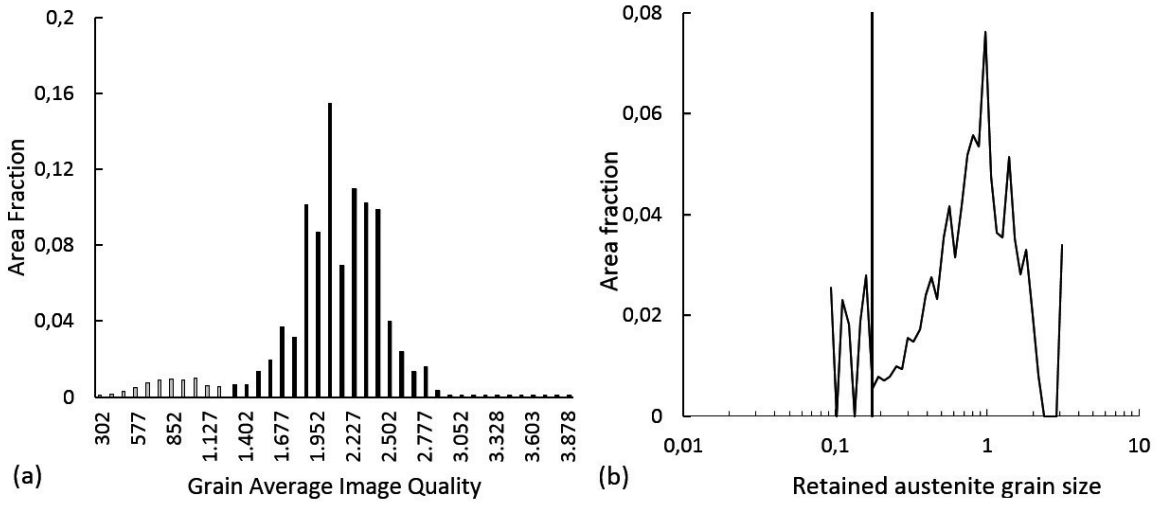

Figure 2. (a) Grain Average Image Quality Distribution (GAIQ) for HA900 steel. Light grey, low GAIQ distribution (martensite indexed). (b) Retained austenite grain size distribution for HA900. Grain sizes to the left from the bold threshold were not considerate for analysis.

It is possible to calculate the austenite volume fraction after austempering treatment by summation of the retained austenite and martensite volume fractions. Finally, the ratio between martensite and austenite after IB treatment indicates the fraction of austenite transformed into martensite due to cooling. Therefore, it can be considered as a chemical stability index of austenite prior to cooling from austempering treatment.

Tensile tests were performed according to ASTM E8M in a servohydraulic Tinius&Olsen universal testing machine under displacement control at 2 mm/min. Three flat specimens 0.87 mm x 12.5 mm were tested for each case. A Linear Variable Differential Transformer with 50 mm gage length was used to measure displacement. Based on tensile test data, true stress vs. true strain curves were obtained for the homogeneous range.

Strain hardening exponent n was obtained from $\sigma=K\varepsilon^n$ Hollomon relationship. The fitting was done based on true strain vs true stress curves.

3. Experimental results

3.1. Heat treatment study

It was possible to achieve a 1/1 austenite/ferrite proportion in the different steels by varying the time at the intercritical annealing, as the desired proportion was achieved after 10 minutes for F/P steel; instead, for steels HA900 and HA1100 these times were of 90 and 135 minutes respectively. According to Roberts and Mehl [17], the austenite nucleation in ferritic-pearlitic steels is carried out mainly in the ferrite-cementite interphase. Areas with high surface energy, as grain boundaries and interphases, are favorable sites for nucleation, but a concentration gradient is also necessary. At interphases the gradients are larger, and the process is faster. This explains the different times needed in the three steels during intercritical annealing: austenite nucleation was faster in the F/P steel than the ferrite nucleation in the HA steels, due to the presence of interphase surfaces and higher carbon concentration gradients in the F/P steel. The ferrite formation for HA900 steel was slightly faster than in HA1100 steel because homogenized austenite in HA900 was finer than in HA1100 (Table 1), showing more grain boundaries and then, more nucleation sites.

3.2 Microstructural characterization

3.2.1 Charactetization by Optical Microscopy, SEM and X-RAY.

Fig. 3 shows the microstructures of the material before and after heat treatment. The microstructure before heat treatment is 42% cold rolled ferrite and pearlite. (Fig. 3a), while the microstructure after heat treatments of F/P, HA900 and HA1100 are shown in Fig 3b, 3c and 3d respectively. LePera etching reveals ferrite in light brown, bainite in dark brown and austenite/martensite phases appear as small white units. Another relevant aspect is the noticeable different morphology between the three microstructures. While the HA900 (Fig. 3c) shows the finest structure, the HA1100 (Fig. 3d) exhibits the coarsest. The ferritic grain diameters and ferrite volume fraction obtained by light optical microscopy are shown in Table 2. Fig. 4 shows SEM micrographs where the different microstructures can be observed: austenite and/or martensite (A/M), ferrite (F) and bainite (B) that appear near or inside prior austenite blocks. This figure confirms that HA1100 steel has the coarsest microstructure, while F/P shows the finest prior-austenite grain size.

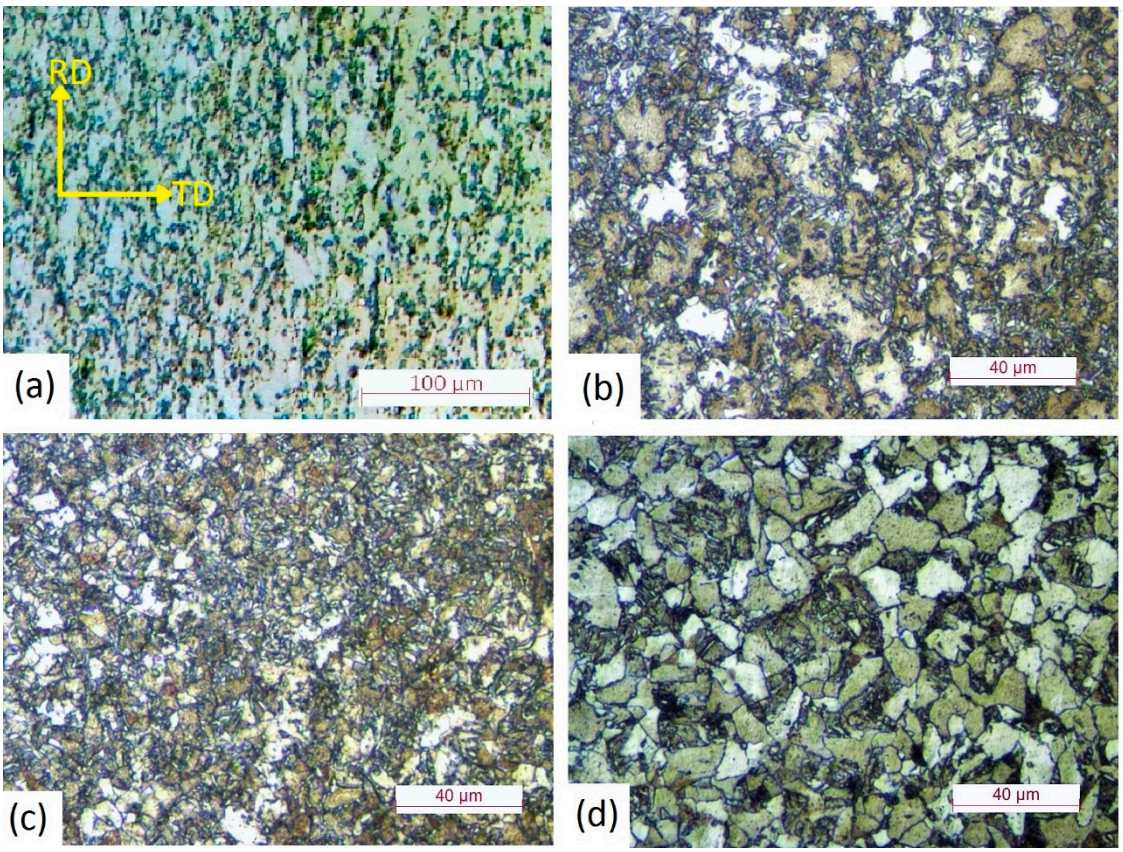

Figure 3. Microstructures: (a) Ferrite and pearlite cold worked, Nital; (b) F/P, LePera; c) HA900, LePera; d) HA1100, LePera. b), c) and d) show three multiphasic TRIP steel low alloy microstructures with noticeably differences in morphologies.

Table 2. Ferrite volume fraction and grain size average.

Steel Id	**F/P**	**HA900**	**HA1100**
Ferrite grain size [µm]	9 ± 4	8 ± 3	11 ± 2
$V_{ferrite}$ [%]	44	45	46

Table 3 summarizes the retained austenite volume fraction obtained from the X-ray analysis and also the estimated carbon content in austenite. Columns 4 and 5 display absolute and relative amounts of transformed retained austenite. Absolute amount is the austenite volume fraction transformed on the whole material and relative amount represents the fraction of transformed austenite referred to initial retained austenite amount. The retained austenite volume fraction was determined by two different ways: X-ray and EBSD (see Tables 3 and 4 respectively), where it is possible to appreciate a good accuracy between both methods. HA1100 steel exhibits the lowest amount of retained austenite.

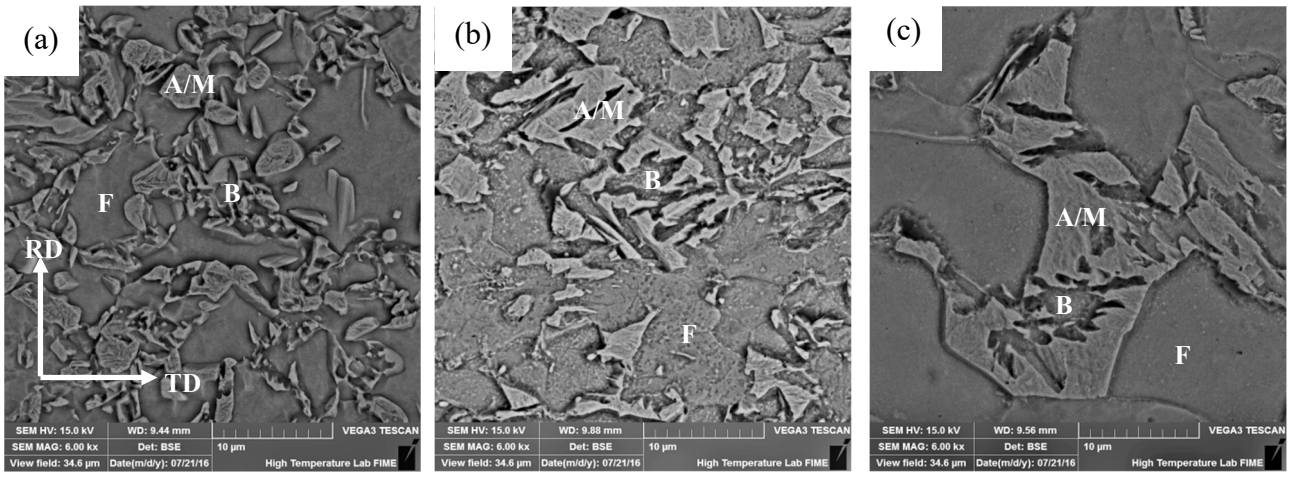

Figure 4. SEM micrographs of representative samples of each steel. (a) F/P, (b) HA900, (c) HA1100. A/M: Austenite/Martensite, F: Ferrite, B: Bainite.

Table 3 Retained austenite volume fraction obtained by X-ray.

Steel Id	% Aust. BTT*	% Aust. ATT**	Transf. Aust.	Transf. Aust. %	%C Ret. Aust.
F/P	5.7	2.2	3.5	62	1.11
HA900	5.0	0.5	4.4	89	0.97
HA1100	3.7	0.4	3.4	90	1.07

* Before Tensile Test

** After Tensile Test

3.2.2 Retained austenite and martensite characterization by EBSD.

Table 4 shows selected morphological characteristics (grain size, aspect ratio, retained austenite and martensite fraction) for each steel. Austenite grain size and aspect ratio are listed in Table 4 and Fig 5 shows IQ + phase map for each steel . As there are no important differences in aspect ratios, this parameter cannot be related to the variations in retained austenite stability. The F/P steel showed the smallest retained austenite grain size, while HA steels exhibited larger grain sizes but with similar values despite of the different prior austenite grain sizes.

Table 4. Characteristics of retained austenite obtained by EBSD.

steel id	F/P	HA900	HA1100
grain size [μm]	0.7 ± 0.3	1.0 ± 0.6	1.0 ± 0.5
aspect ratio	2.7 ± 1.6	2.6 ± 1.3	2.9 ± 1.6
RA vol. fraction %	5.9	5,3	3.5
martensite vol. fraction %	2.5	4.1	4.8
aust. after IB treatment %	8.4	9.4	8.3
aust. transf. to martensite by cooling from IB %	30.0	43.6	57.8

Preprints (www.preprints.org) | NOT PEER-REVIEWED | Posted: 5 November 2018 doi:10.20944/preprints201811.0104.v1

Peer-reviewed version available at Metals 2018, 8, 1021; doi:10.3390/met8121021

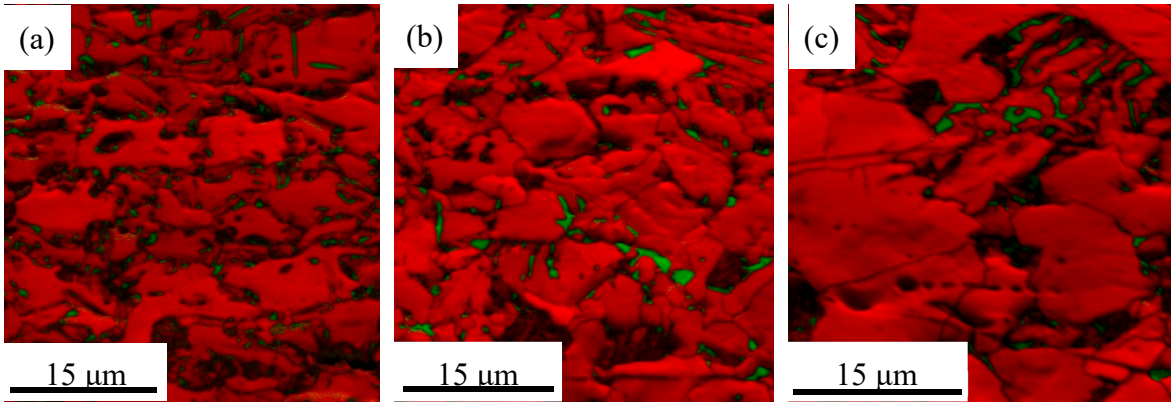

Figure 5. IQ + phase map for each steel. Due to IQ map, dark zones correspond to low IQ value, and due to phase map, in red BCC structures (ferrite, bainite, martensite), green FCC structures (austenite). (a) F/P steel, (b) HA900 steel, (c) HA1100 steel. Step size 60 nm.

3.3 Texture Analyses

Fig. 6 shows the Orientation Distribution Function (ODF) for the BCC structures (mainly ferrite and bainite) in each steel. Fig. 6a shows the key for the main orientations in BCC iron. Fig. 6 also shows that, in all cases, there is a maximum intensity on {554}<225> and {112}<110>, and variants near to them like {332}<113> and {111}<112> or {113}<110> and {223}<110>. It is known that {554}<225> promotes good drawing properties while {112}<110>is not good for drawing properties [18]. On the other hand, HA steels exhibited a considerable wide range of variants related to {001}<110> texture. Although the three steels exhibit α and γ fibre components, it is noticeable that they are more intense in F/P steel.

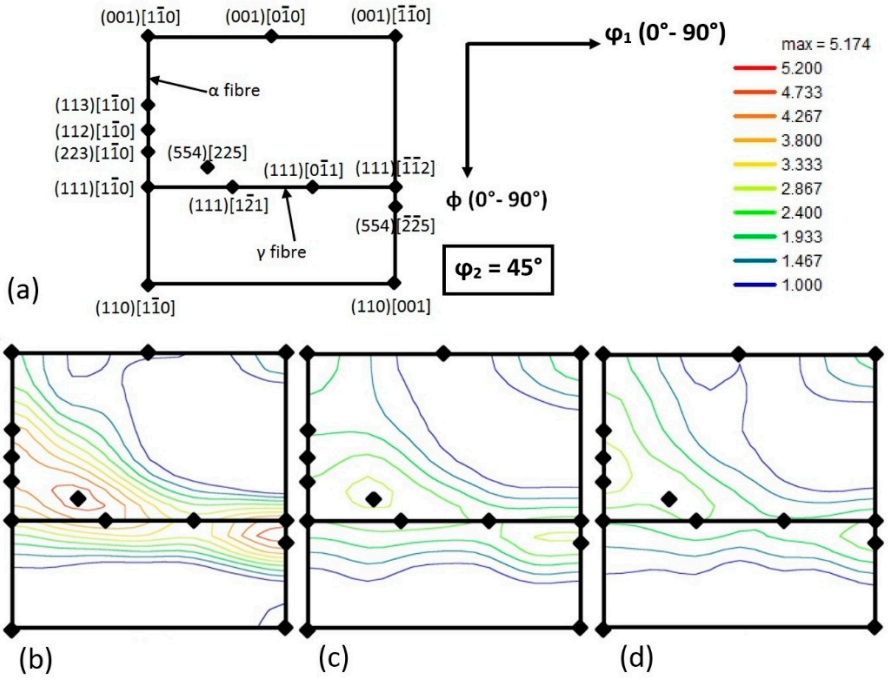

Figure 6. (a) ODF map with exact positions of important orientations for bcc structures in steel, Euler space (ϕ_2=45°) section. (b), (c) and (d) Euler space section of the ODF of the constituents with bcc structures for each steel at same intensity scale (ϕ_2=45°), F/P, HA900 and HA1100 respectively. Bunge notation. Intensity in mrd (multiple of random density).

Retained austenite ODF map for F/P steel (Fig. 7b) shows the maximum intensity for Brass, Goss, Copper and Rotated Goss fibre components. Several authors [18,19] have shown that Copper texture ({112}<111>) generates {113}<110> (and near variants like {112}<110>) in BCC structures due to the Kurdjumov-Sachs K-S relationship, while Brass texture ({110}<112>) promotes {332}<113> (and near variants like {554}<225>). On the other hand, Goss texture ({110}<001>) generates {111}<110> and {112}<110> BCC textures. From these results α and γ fiber textures are expected.

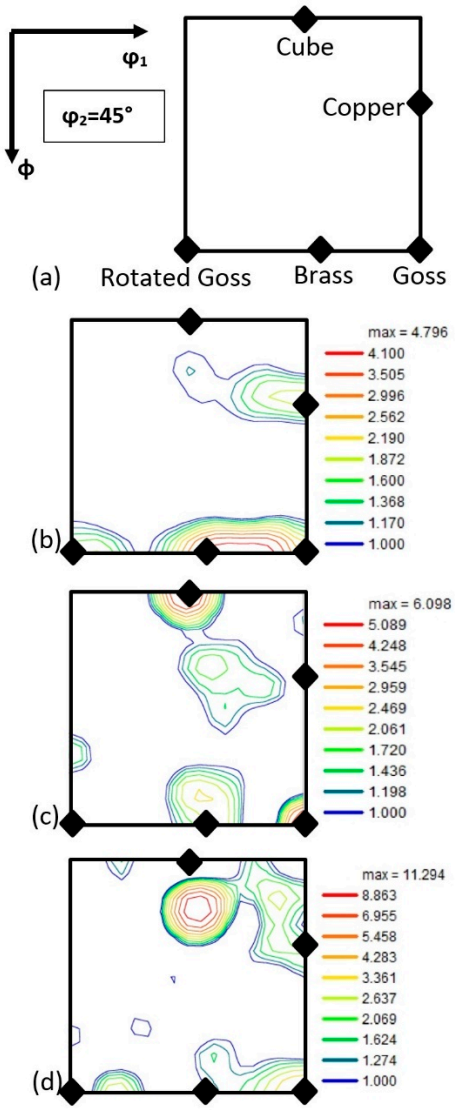

Figure 7. (a) Exact position of the most important austenite texture components on Euler space section φ_1=(0°,90°), ϕ=(0°,90°) and φ_2=45°. (b), (c) and (d): Retained austenite ODF maps of F/P, HA900 and HA1100 respectively. Bunge notation. Intensity on mrd.

Some authors [18,20] have shown that {112}<110> ferrite texture component increases significantly with cold-rolling, which means that the initial material, proeutectoid ferrite 42% cold-rolled, has a strong {112}<110> texture component. Ray and Jonas [18] have also indicated that at ferrite with {112}<110> texture recrystallizes into {554}<225>, which means that during intercritical annealing, ferrite F/P steel would develop a strong {554}<225> texture component. Summarizing, a strong α and γ fibres components BCC textures are expected in F/P steel due to austenite developed and ferrite recrystallization during intercritical annealing treatment at 750°C.

For HA steels, BCC textures must be related to homogenized austenite textures at 900 and 1,100°C respectively. It is expected that retained austenite must inherit its texture from homogenized

austenite. Retained austenite ODF maps for HA900 and HA1100 are shown in Fig. 7c and 7d respectively.

Retained austenite in HA900 steel shows maxima in Cube and Goss textures and also a wide range of variants related to {110}<112> Brass texture. Cube texture promotes Rotated Cube texture {001}<110> [19]. Brass texture, as was mentioned previously, generates {332}<113> (and near texture variants), and in less grade, Brass texture can also transforms into Rotated Cube variants. In the current case, the main BCC texture components observed for HA900 (Fig. 6c) were inherited from Brass and Cube prior austenite texture.

Retained austenite in HA1100 exhibited a maximum close to Cube position, and it could be related to {001}<110> texture variants observed on HA1100 ODF map of BCC structure (Fig. 6d). It is also shown Fig 6d that the retained austenite exhibits variants close to Goss and Copper texture components, which are related to α and γ fibres.

According to Ray and Jonas [18] there is an effect of the temperature above A_3 (and then, the austenite grain size) on deformation textures of ferrite: {332}<113> component in ferrite is strengthened noticeably when the initial austenite grain size is small (heated slightly above A_3), while {113}<110> remains insensitive to austenitic grain size. This result is in agreement with the current research, in the sense that {554}<225> component, which comes from {332}<113>, is strong for HA900 steel (austenized at low temperature).

Based on scale map of BCC structures (Fig. 6), in F/P steel the maximum intensity for components related to γ fibre is 5.2 multiple of random density (mrd), in HA900 steel is 2.9 mrd and in HA1100 steel is 2.5 mrd. For HA steels, the intensity of Rotated Cube components is higher than F/P, it means that the ratio between γ fibre and Rotated Cube is higher for F/P steel. Due to this facts, is expected that F/P steels will have a better deep drawing behavior than HA steels, provided that there are no other disturbing constituents in the microstructure.

3.4 Retained austenite stabilization

3.4.1 Mechanical stability

Mechanical stability was evaluated measuring the austenite volume fraction transformed into martensite due to tensile testing. These results are shown in Table 3. F/P steel exhibit less relative transformation than HA steels. This implies that retained austenite is more stable in F/P steel. These results, together with the austenite grain sizes shown in Table 4 are in accordance with other authors [6,7]: the coarser the retained austenite, the lower its stability. Both HA steels presented similar retained austenite grain size and, in both cases, the residual austenite volume fraction, after tensile testing, was near to zero. Although it is difficult to compare the mechanical stability between HA steels, the main conclusion is, that retained austenite was unstable and prone to transform into martensite during deformation.

3.4.2 Chemical stability

The chemical stability was measured by the fraction of austenite transformed into martensite during cooling from austempering treatment. These results are shown in Table 4. Clearly, the austenite in F/P steel is the most stable. Although HA steels exhibits a similar mechanical stability, there is an important difference in chemical stability. Due to the coarser prior austenite, the HA1100 steel presents the less stable austenite. This instability comes from the larger defect density associated to a larger grain size [8] and then, a higher number of available sites for martensite nucleation.

3.5 Mechanical properties

Tensile tests results are summarized in Table 5. Fig. 8 shows true stress v/s true strain curves in the homogeneous deformation range. As the austenite in F/P steel is with the highest chemical stability, there is a low amount of austenite-martensite transformation by cooling from austempering, and then, a lower dislocation increment in the ferrite matrix due to Greenwood-

Peer-reviewed version available at Metals 2018, 8, 1021; doi:10.3390/met8121021

Johnson [21] effect (dislocations increment on ferrite matrix due to volume accommodation by austenite martensite transformation). So, ferrite of F/P steel exhibits a lower hardening by this way, and then, a larger straining capacity. In order to understand the elongation improvement of F/P steel, it is necessary to mention that these materials are constituted by ferrite, bainite, austenite and martensite, with ferrite (a soft constituent) and bainite (hard constituent) present in similar proportion, although in larger amount than austenite and martensite. So, it is expected that ferrite must be the constituent with most contribution to the total strain. Then, F/P steel exhibits the highest plastic deformation due to the lowest hardening that ferrite experiments by austenite transformation.

HA steels exhibit a similar UTS and elongation behavior although noticeable microstructural differences. HA1100 presents the highest YS and HA900 steel has the highest work hardening exponent. The highest *n* value for HA900 steel can be due to the greater absolute amount of retained austenite transform into martensite by plastic strain and its finest microstructure. F/P steels show the lowest UTS due to the low fraction of austenite transformed into martensite in both ways: after cooling from austempering and under plastic strain.

Table 5. Mechanical properties (average of three tests).

Steel id	UTS [MPa]	YS [MPa]	EL [%]	hardening index *n*
F/P	385 ± 27	732 ± 13	22.7 ± 2.0	0.19 ± 0.00
HA900	401 ± 39	787 ± 23	16.8 ± 0.7	0.22 ± 0.01
HA1100	438 ±16	796 ± 8	16.3 ± 1.7	0.20 ± 0.00

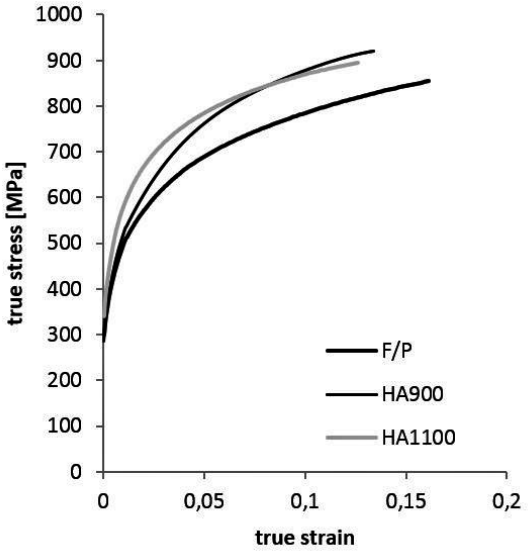

Figure 8. (a) True stress v/s true strain curves.

4. Conclusions

Heat treatments were performed to obtain similar α/γ fractions after intercritical annealing treatment from three different microstructures: ferrite/pearlite and homogenized austenite with two different prior grain sizes 10.3 μm and 18.9 μm. This allowed to relate microstructural characteristics with austenite stability and mechanical properties. The most important findings can be summarized as follows:

- A change from 900 to 1100°C in the homogenization temperature of austenite does not exert an effect on the retained austenite grain size, but it affects the prior austenite grain size and the austenite chemical stability. At homogenization temperature of 1100°C, the chemical stability is lower (higher M_S) than after homogenization of 900°C and a higher amount of austenite transforms into martensite after cooling from the austempering treatment.

- The homogenized at 1100 and 900°C steels exhibit the highest UTS value. This is related to the austenite martensite transformation which induces an extra dislocation increment and consequently, a high strength.

- Extra dislocation increment also decreases the strain ability, so the homogenized steels exhibit lower elongation than the ferrite-pearlite steel.

- The global mechanical response is also related to the surrounding phases. Thus, the steel homogenized at 900 °C exhibits the highest strain hardening index, due to its finest microstructure.

- An austenization treatment at elevated temperature increases the yield strength. The steel homogenized at 1100 °C exhibits the highest YS despite its coarsest microstructure.

- A ferrite pearlite cold rolled initial microstructure promotes better texture components for deep drawing process than homogenized austenite initial microstructure. For HA initial microstructure, a lower homogenization temperature promotes γ fibre components.

Acknowledgments

The authors wish to thank to "Proyectos Basal USA 1555 - Vridei 051714MG_MOV. Universidad Santiago de Chile", FONDECYT Grant 1170905, CONICYT-PFCHA/Doctorado Nacional/2013-21130833 and DICYT USACH for the economic support.

References

1. Petrov, R.; Kenstens, L.; Houbaert, Y. Recrystallization of a cold rolled TRIPtrip-assisted steel during reheating for intercritical annealling. *ISIJ Int.* **2001** *41*, 883-890, DOI: 10.2355/isijinternational.41.883.
2. Jacques, P.J; Furnémont, Q.; Lani, F.; Pardoen, T.; Delannay, F. Multiscale mechanics of TRIP-assisted multiphase steels: I. Characterization and mechanical testing. *Acta Mater*. **2007** *55*, 3684-3693, DOI: 10.1016/j.actamat.2007.02.029.
3. Van Dijk, N.H.; Butt, A.M.; Zhao, L.; Sietsma, J.; Offerman, S.E.; Wright, J.P.; Van der Zwaag, S. Thermal stability of retained austenite in TRIP steels studied by synchrotron X-ray diffraction during cooling. *Acta Mater*. **2005** *53*, 5439-5447, DOI: 10.1016/j.actamat.2005.08.017.
4. Zrník, J.; Muránsky, O.; Lukáš, P.; Nový, Z.; Sittner, P.; Horňak, P. Retained austenite stability investigation in TRIP steel using neutron diffraction. *Mater. Sci. Eng. A*, **2006** *437*, 114-119, DOI: 10.1016/j.msea.2006.04.067.
5. Van Der Zwaag, S.; Zhao, L.; Kruijver, S.O.; Sietsma, J. Thermal and mechanical stability of retained austenite in aluminum-containing multiphase TRIP steels. *ISIJ Int.* **2002** *42*, 1565-1570, DOI: 10.2355/isijinternational.42.1565.
6. Basuki, A.; Aernoudt, E. Influence of rolling of TRIP steel in the intercritical region on the stability of retained austenite. *J. Mater. Process. Technol.* **1999** *89-90*, 37-43, DOI: 10.1016/S0924-0136(99)00037-0.
7. Wang, X.D.; Huang, B.X.; Rong, Y.H.; Wang, L. Microstructures and stability of retained austenite in TRIP steels. *Mater. Sci. Eng. A*. **2006** *438–440*, 300-305, DOI: 10.1016/j.msea.2006.02.149.

8. Chatterjee, S. Transformations in TRIP-assisted Steels: Microstructure and Properties. Ph.D. thesis, Cambridge University, 2006.
9. Sugimoto, K.; Usui, N.; Kobayashi, M.; Hashimoto, S. Effects of volume fraction and stability of retained austenite on ductility of TRIP-aided dual-phase steels. *ISIJ Int*. **1992** *32*, 1311-1318, DOI: 10.2355/isijinternational.32.1311.
10. Pereloma, E.V.; Timokhina, I.B.; Miller, M.K.; Hodgson, P.D. Three-dimensional atom probe analysis of solute distribution in thermomechanically processed TRIP steels. *Acta Mater.* **2007** *55*, 2587-2598, DOI: 10.1016/j.actamat.2006.12.001.
11. De Cooman, B.C. Structure–properties relationship in TRIP steels containing carbide-free bainite. *Curr. Opin. Solid State Mater. Sci.* **2004** *8*, 285-303, DOI: 10.1016/j.cossms.2004.10.002.
12. Guzmán, A. Obtención y estudio de las propiedades mecánicas y microestructurales de un acero con comportamiento TRIP (0,21%C, 0,82%Si, 1,87%Mn y 0,43%Al). Phd. Thesis, Universidad de Santiago de Chile, 2012.
13. Matsumara, O.; Sakuma, Y.; Takechi, H. Enhancement of elongation by retained austenite in intercritical annealed 0.4C-1.5Si-0.8Mn steel. *Trans. ISIJ*. **1987** *27*, 570-579, DOI: 10.2355/isijinternational1966.27.570.
14. Roberts, C.S.; Effect of carbon on the volume fractions and lattice parameters of retained austenite and martensite. *J. Met.* **1953** *197*, 203-204.
15. Ryde, L. Application of EBSD to analysis of microstructures in commercial steels. *Mater. Sci. Technol.* **2006** *22*, 1297-1306, DOI: 10.1179/174328406X130948.
16. Petrov, R.; Kestens, L. Advanced high-strength steels: Electron Backscattering diffraction (EBSD), In *Encyclopedia of Iron, Steel and Their Alloys*; Colás, R., Totten, G.E., Eds.; CRC Press: Boca Ratón, FL, USA, 2016; pp. 46-69, DOI: 10.1081/E-EISA-120050786.
17. Roberts, G.A.; Mehl, R.F. The mechanism and the rate of formation of austenite from ferrite-cementite aggregates. *Trans. ASM*. **1943** *31*, 613–650.
18. Ray, R.K.; J.J. Jonas, J.J. Transformation textures in steels. *Int. Mater. Rev.* **1990** *35*, 1-36, DOI: 10.1179/095066090790324046.
19. Butrón-Guillén, M.P.; Jonas, J.J.; Ray, R.K. Effect of austenite pancaking on texture formation in a plain carbon and a Nb microalloyed steel. *Acta Metall. Mater*. **1994** *42*, 3615-3627, DOI: 10.1016/0956-7151(94)90428-6.
20. Hutchinson, B. Deformation microstructures and textures in steels. *Philos. Trans. R. Soc. Lond. A.* **1999** *357*, 1471-1485, DOI: 10.1098/rsta.1999.0385.
21. Greenwood, G.W.; Johnson, R.H. The deformation of metals under small stresses during phase transformations. *Proc. R. Soc. Lond. A* **1965** *283*, 403-422, DOI: 10.1098/rspa.1965.0029.